Surfaces and Interfaces 58 (2025) 105849

Contents lists available at ScienceDirect

Surfaces and Interfaces

journal homepage: www.sciencedirect.com/journal/surfaces-and-interfaces

Black anatase-TiO_2 electrodes for sun-activated photocatalytic degradation of organic water contaminants

Jaime A. Benavides-Guerrero [a], Paul Fourmont [a,b], Luis Felipe Gerlein [a], Astrid C. Angel-Ospina [a], Fiderman Machuca-Martinez [c], Fabrice Vaussenat [a], Caroline A. Ross [b], Sylvain G. Cloutier [a,*]

[a] Department of Electrical Engineering, École de Technologie Supérieure, 1100 Notre-Dame West, H3C 1K3, Montreal, QC, Canada
[b] Department of Materials Science and Engineering, Massachusetts Institute of Technology 77 Massachusetts Ave, Cambridge, MA 02139, United States
[c] Escuela de Ingeniería Química, Universidad del Valle, Calle 13 # 100-00, Santiago de Cali, Colombia

ARTICLE INFO

Keywords:
Black TiO_2
Oxygen vacancies
Visible light
Photocatalysis, sol-gel

ABSTRACT

This study presents the synthesis of black anatase in air and its use for the fabrication of a reusable electrode for the photocatalytic degradation of Rhodamine B (RhB) under visible-light. Characterization techniques such as X-ray diffraction, Raman spectroscopy, and Transmission Electron Microscopy (TEM) were used to analyze the properties of black anatase. The immobilization of black TiO_2 on a glass substrate eliminates the need for post-treatment recovery of the photocatalyst. Enhancement of photocatalytic activity was achieved by depositing a 4 nm platinum layer on the black anatase TiO_2 electrode. Activation of the photocatalytic process ($\lambda \geq 400$ nm) was conducted with a solar simulator, and the degradation of RhB was monitored through visible absorption and time-resolved fluorescence spectroscopy, revealing degradation efficiencies of 94 % and 89 % after 40 and 60 min, respectively. These results are attributed to the elevated levels of oxygen vacancies and the Schottky barrier formed between the platinum layer and black anatase. The methodology's simplicity and the significant photocatalytic efficiency suggest potential for widespread application in solar-driven photocatalytic degradation.

1. Introduction

Photocatalytic processes have attracted attention because they offer environmental benefits, while being relatively inexpensive and capable of yielding high efficiencies [1]. These processes can treat hazardous effluents, such as polychlorinated biphenyls and cyanide solutions, with degradation efficiencies approaching 100 % [2,3], and suggesting photocatalysis as an effective and viable technique for indoor and outdoor pollution control [4]. Photo-induced catalysis also offers several advantages over other catalytic processes. First, the reaction can occur under normal ambient conditions using natural sunlight, room temperature, and atmospheric pressure [5]; Second, the process is also pollution-free [6],which reinforces the drive for low-carbon environmental protection initiatives [6]. Lastly, using inexpensive, nontoxic and recyclable photocatalysts [7] makes it particularly attractive for industrial implementations [8].

Metal-oxide semiconductors are often favored as photocatalyst materials, thanks to their photo-corrosion resistance and biocompatibility [9]. Some examples of photocatalyst materials include Fe_2O_3 [10], $SrTiO_3$ [11], ZnO [12], WO_3 [13], ZrO_2 [14], $BiFeO_3$ [7,15], and standard (so-called white) TiO_2 [16]. These materials exhibit a spectrum of efficiencies in degrading organic pollutants; for instance, Fe_2O_3 has been reported to remove up to 90 % of certain dyes under visible light [17], while $SrTiO_3$ has shown a 51 % removal rate for Acid Orange 7 after ultraviolet exposure [18]. The combination of ZnO with graphene oxide has resulted in a remarkable 95 % degradation of methyl blue [19], and carbon-doped WO_3 has similarly achieved a 95 % reduction in Methyl Orange concentration [20]. Although ZrO_2's photocatalytic activity is somewhat limited, doping with neodymium has significantly enhanced its performance, achieving an 80 % degradation rate [21]. $BiFeO_3$, on the other hand, has demonstrated a remarkable 93 % efficiency in degrading RhB [7].

Despite these advancements, challenges persist, such as the rapid recombination of photogenerated charge carriers and the inherently wide bandgaps of these materials, which limit their absorption of visible light. Consequently, modifications, typically through doping or the

* Corresponding author.
E-mail address: sylvaing.cloutier@etsmtl.ca (S.G. Cloutier).

https://doi.org/10.1016/j.surfin.2025.105849
Received 29 May 2024; Received in revised form 26 December 2024; Accepted 15 January 2025
Available online 15 January 2025

formation of composites, are often required to overcome these limitations.

Of all of them, TiO_2 is possibly the most extensively studied, largely due to its ability to break down organic pollutants and achieve complete mineralization [22]. However, standard white-TiO_2 has a wide band gap which makes it photocatalytically active in the UV-range. In spite of this, its excellent chemical stability makes it resistant to corrosion and degradation, while is non-toxic and biocompatible [16]. TiO_2 has also a tunable bandgap, enabling extended light absorption into the visible spectrum [23], and it can be synthesized in various nanostructures, enhancing its surface area and reactivity [24].

In general, the photocatalytic degradation process consists of four steps: (1) photo-excitation of charge carriers, (2) carrier migration to the catalyst surface, (3) formation of radicals at the surface, and (4) redox reactions with the environment [25]. To promote such reactions, the excitation source must match or exceed the semiconductor bandgap to favor photo-excited carrier generation [26]. These photo-generated carriers then participate in the redox reactions at the interface between the photocatalyst and the environment [27]. To enhance reaction efficiency and reduce carrier recombination, the photocatalyst should ideally be a porous nanostructure, allowing photo-generated carriers to reach the surface quickly [7,27]. Nanostructured materials benefit from large surface areas and high surface defect densities offering exceptional properties for applications in surface science, catalysis, electronics, biomedical fields, and energy technologies [28]. Regarding TiO_2 as a photocatalyst, nanostructures provide more active sites for the adsorption of reactant molecules, increasing the chances of photocatalytic reactions occurring [29]; Meanwhile, surface defects can act as trap states for photo-generated charge carriers, extending their lifetime, and facilitating the transfer of electron-hole pairs, thereby enhancing activity in the visible spectrum [30].

In its crystalline forms, TiO_2 has a bandgap of 3.0 eV for rutile [31], 3.2 eV for anatase, and 3.1–3.4 eV for brookite [32]. However, for photocatalysis, it typically requires UV light for activation [33]. Since UV light represents only ~4 % of the total sun irradiance, this hinders TiO_2 large-scale deployment [29]. To address this limitation, bandgap engineering of TiO_2 has been explored initially using different metallic [34–36] and non-metallic [37–39] dopants, which helped on tuning the properties of TiO_2 at atomic scale and extend light absorption into the visible spectrum [40]. Latter strategies included self-doping [41,42] during 2010s, with black hydrogenated TiO_2 with enhanced solar absorption[43]. More recently, defect engineering in TiO_2, particularly through oxygen-vacancy engineering, has shown promising results in improving visible light absorption [44,45].

Heating TiO_2 under vacuum [46,47,47], in a reducing atmosphere [43,46,48], or with reductive agents [49] is known to cause color changes in TiO_2, resulting in a *gray* or *black* color with significantly enhanced visible light absorption [40,50,51]. The shift from the standard white to gray or black TiO_2 is largely attributed to the formation of Ti^{3+} defects and oxygen vacancies [31,44,52,53], which introduce deep electronic defect states located between 0.75 and 1.18 eV below the conduction band [30,54], and increase visible light absorption of TiO_2 [31,55]. Oxygen vacancies, common surface defects in metal oxides [56], play a crucial role in tuning the electronic and redox properties of metal oxides, which is critical for heterogeneous catalysis [57]. These vacancies trap one or two electrons and create unsaturated surfaces with a lower coordination number and dangling Ti bonds [58,59]. This enhances photocatalytic degradation by promoting the charge separation process [54,60], and providing sites for co-catalyst deposition [61,62]. Additionally, oxygen vacancies are well characterized in TiO_2 as electron donors that boost the catalyst donor density, improves the charge transport, and shift the Fermi level towards the conduction band, facilitating the charge separation process [54].

In this article, the unique photo-catalytic properties of *black* anatase-TiO_2 synthesized from an oxygen-deficient amorphous TiO_2 formulation developed first in [45] through a simple chelated sol-gel process followed by thermal crystallization in air, were reported and tested for photocatalytic RhB degradation. Typical synthesis methods for black TiO_2 are often time-consuming [63] and require high temperatures and pressures [43], vacuum [64], or reducing atmospheres such as N_2, H_2, or Ar, which significantly raise the cost of large-scale industrial production [43,46,65,66]. Therefore, in this study we have demonstrated a promising strategy for synthesizing black TiO_2 in air. This oxygen-deficient crystalline black TiO_2 was characterized by electron paramagnetic resonance (EPR), X-ray diffraction (XRD), Raman and UV–vis spectroscopy, Transmission Electron Microscopy (TEM) and Scanning Electron Microscopy (SEM). The electrode composition was analyzed by Energy Dispersive X-ray Spectroscopy (EDS) and X-ray Photoelectron Spectroscopy (XPS) for determining oxygen-vacancy concentration. Following characterization, visible light photocatalysis was achieved using black TiO_2 electrodes coated with a 4 nm-thick platinum (Pt) layer. These reusable electrodes achieved 94 % degradation of RhB in only 40 min for the first cycle, and 89 % degradation in 60 min for the second cycle. Finally, the degradation mechanism kinetics were investigated using transient absorption spectroscopy.

2. Experimental section

2.1. Synthesis of amorphous oxygen-deficient TiO_2

Oxygen-deficient amorphous TiO_2 was prepared following a modified sol–gel synthesis described elsewhere [45]. To do so, 28.8532 g of ethanol (Product 1,590,102,500 from Sigma-Aldrich) were mixed with 1.4748 g of acetylacetone (Product P7754–1L-A from Sigma-Aldrich). This solution was stirred for 20 min. Subsequently, 10.8604 g of titanium (IV) butoxide (Product 244,112–500 G from Sigma-Aldrich) were added and stirred for 40 min. Finally, the hydrolysis reaction was triggered by adding 0.84 mL of deionized water. The sol-gel formulation was agitated for 120 min and then aged for 8 months to yield amorphous red vacancy-rich TiO_2. The ethanol slowly evaporates during aging period to precipitate an amorphous red vacancy-rich TiO_2 powder [45]. The Table S1 summarize all the quantities used in this synthesis.

2.2. Synthesis of black anatase-TiO_2

Amorphous red vacancy-rich TiO_2 powder was placed in a crucible at 450 °C for 90 min to obtain black vacancy-rich TiO_2 powder (see Fig. 1 (b)) following the temperature ramps shown in Fig. 1(c). At the 90 min mark, the crucible was removed from the oven and allowed to cool to room temperature for an additional hour. Removing the TiO_2 crucible is a critical step since oxygen vacancies diffuse and bleach out if they are left for prolonged times at high temperatures [30].

2.2.1. Black anatase characterization

EPR measurements were performed using a Bruker Magnettech ESR5000 at 9.45618 GHz. XRD patterns were obtained on a XRD X'Pert Panalytical using a Cu Kα X-ray source to characterize the crystallinity and phase of the defective black anatase-TiO_2. Confirmation of the crystalline structure and the presence of defects were assessed through Raman spectroscopy. This analysis was done using a WITEC Alpha300 confocal Raman microscope, which is equipped with a 532 nm laser and a power output of 60 mW. Optical absorption was measured using a UV–vis-NIR spectrophotometer (PerkinElmer, LAMBDA 750) with an integrating sphere to capture diffuse light. TEM (Jeol, JEM-2100F) equipped with an electron energy loss spectrometer, SEM (Hitachi, SU8230) and an EDS detector (Bruker, QUANTAX FlatQUAD) were used to characterize morphology and perform elemental mapping. Imagej v1.54g software was used to calculate the interplanar distance in the obtained TEM images. XPS was performed using a Thermo Fisher Scientific Escalab 250Xi instrument equipped with a monochromated Al Kα radiation source (218.8 W, 14.7 kV, 14.9 mA) and a 180° hemispherical analyzer in constant energy mode. A standard charge neutralization

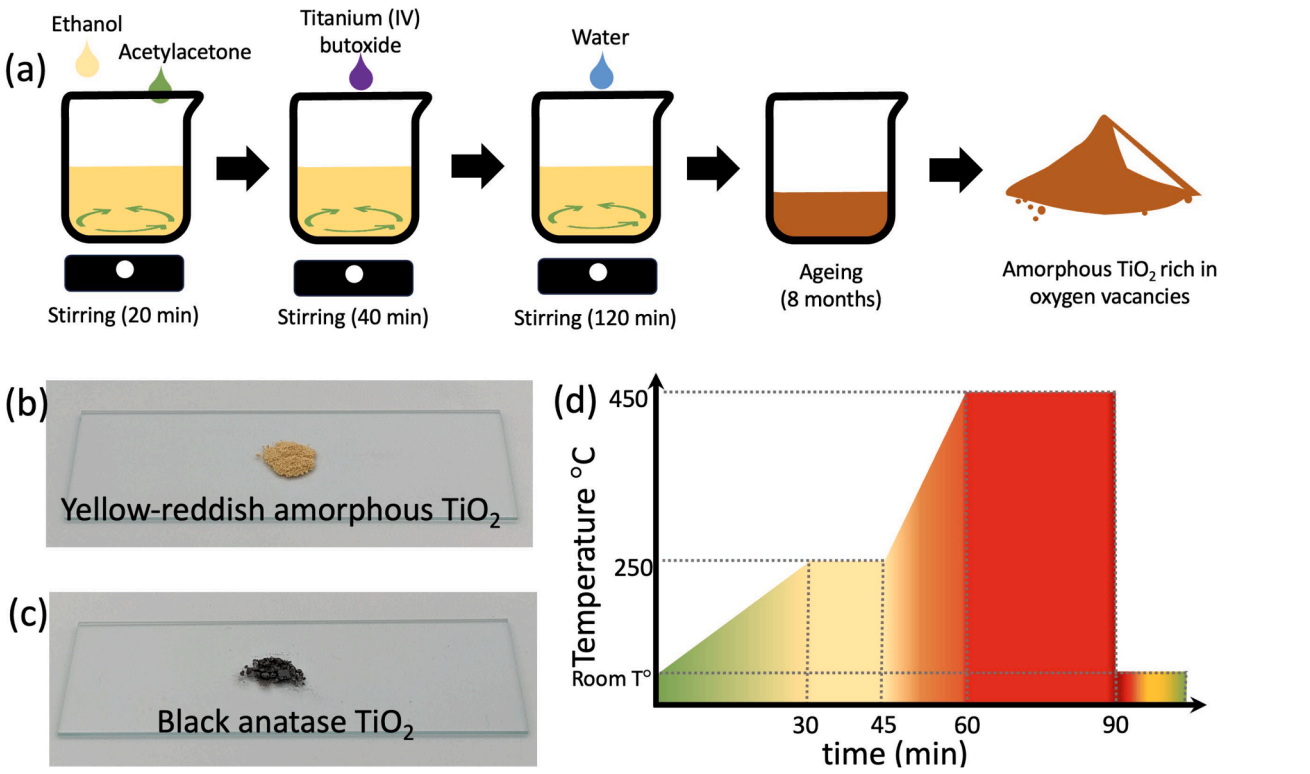

Fig. 1. (a) Schematic representation of the synthesis process. (b) Amorphous TiO_2 powder before thermal treatment. (c) Crystallized anatase TiO_2 powder after thermal treatment. (d) Schematic representation of the thermal treatment used to crystallize the TiO_2 powder.

system consisting of low energy electrons and Ar^+ ions was applied, maintaining a base pressure of ~10^{-8} mbar. Survey scans were recorded with a pass energy of 150 eV and an energy step of 1.0 eV, while high resolution scans were performed with a pass energy of 20 eV and an energy step of 0.1 eV The samples were oriented at a 0° emission angle, which corresponds to an XPS probing depth of 5–10 nm for a flat surface. Data analysis was performed using Avantage v6.5.0 software (Thermo Fisher Scientific), with elemental composition (excluding H and He, which are not detectable by XPS) obtained from the survey scans by integrating the peak areas and applying the sensitivity factors provided by the instrument manufacturer. The binding energy scale was calibrated by setting the C1 s peak at 285.0 eV for aliphatic hydrocarbons.

2.3. Construction of the black anatase and Degussa P25 electrodes for photocatalysis

Black anatase-TiO_2 is supported on a glass substrate of 25 mm x 25 mm. First, the glass substrate was cleaned with acetone, ethanol, and DI water. Afterwards, we spin coated SOL725 (Henkel) at 200 rpm for 30 s on top of the glass substrate. Then, we deposited 300 mg of the black anatase powder on top of the SOL725 rm. The dispersion process was repeated three times to ensure complete and even coverage of the entire area. Excess of black anatase-TiO_2 powder was removed by shaking the electrode, followed by curing at 125 °C for 1 hour. The same procedure was used to fabricate the Degussa P25 electrode.

2.4. Photocatalytic test measurements and degradation kinetics

RhB was selected as the target contaminant to evaluate the photocatalytic activity of the prepared electrodes. The solar simulator (Newport, 91160–1000) certified to class AAA, is equipped with a 300 W xenon lamp. The light intensity is calibrated at 100 mW cm^{-2} (1 sun). To ensure the tests were performed only with visible light, a cutoff filter (≥400 nm) was installed right after the AM 1.5 G filter. The RhB solution was placed in a 50 mL beaker under the light beam from the solar simulator and was kept at room temperature to avoid any thermal degradation. A horizontal beam of a tungsten halogen light source (Ocean Optic, HL- 2000-HP, output power 8.8 mW) allowed a live tracking of the RhB signal. To guarantee precise monitoring of the degradation reaction, the absorbance spectrum is recorded every minute in the 400 to 800 nm wavelength range. The spectra are analyzed using Matlab to extract the maximum intensity of absorbance and the peak positions.

RhB solution was prepared from a mother solution with 5 mg L^{-1} concentration (in distilled water) and pH = 6.1. The photocatalyst concentration used in this study falls within the established ranges reported in the literature for immobilized TiO_2 photocatalysis [67,68]. Additionally, the RhB dye concentration is proportional to the absorbance at this concentration range (mg L^{-1}) [7]. For each degradation test, a 25 mL sample was used. The RhB degradation rate and kinetics were then calculated by absorbance measurements, comparing the final absorbance to the initial maximum absorbance at the start of the reaction.

3. Results and discussion

3.1. Chemical reactions that yield black anatase-TiO_2

The sol-gel reaction used to synthesize the black TiO_2 relies on the chelation reaction of titanium butoxide ($Ti(OBu)_4$) by using acetylacetone (acac) as complexation agent [45,69]. An interexchange substitution mechanism is responsible for this reaction and it can be described as follows [69,70]:

$$Ti(OBu^n)_4 + acacH \rightarrow Ti(OBu^n)_{4-x} + xBuOH$$

This modified reaction involves the creation of a hybrid $Ti_{(IV)}$-acetylacetonate compound in which the steric inhibition effect created by the acetylacetonate groups prevents the hydrolyzation of the titanium

precursor and promotes the formation of oxygen deficiency [45,71]. The use of acetylacetonate as a complexing agent in TiO_2 sol-gel systems has been previously reported to yield a very stable photo-responsive black anatase TiO_2 after crystallization in air at 400 °C [72]. The stability of the material relies on the $Ti_{(IV)}$-complex, providing an electronic structure that stabilizes superoxide anion radicals on its surface for long periods of time at room temperature [72,73]. This simple synthesis process is performed entirely at room temperature and does not require harsh conditions or external reducing agents [72,73]. Such characteristics are important to reduce fabrication costs and enable large-scale manufacturing.

This complexation process significantly affects the coloration of the TiO_2 sol-gel system and its products [74]. The schematic representation of the synthesis process is depicted in Fig. 1(a). As shown in Fig. 1(b), the synthesis yields a yellow-reddish colored oxygen-deficient amorphous TiO_2 [45]. However, Fig. 1(c) shows that the powder converts to black anatase TiO_2 after thermally-induced crystallization at 450 °C in air [73]. Fig. 1(d) shows a schematic of the thermal treatment process.

As it will be further demonstrated, black color in the crystallized TiO_2 is directly associated with high concentrations of oxygen vacancies. Its promotion and disappearance during the thermal crystallization can be explained using previous models [30,54], establishing that temperatures between 300 °C and 500 °C promote the entropy-driven outward diffusion of the oxygen vacancies towards the nanoparticle surfaces [30]. However, temperatures higher than 500 °C can generate enough energy to bleach out the surface defects, making the black color fade away due to a decrease in the concentration of oxygen vacancies [30]. Therefore, to preserve the oxygen vacancies and reduce their diffusion it was important to limit the annealing time of the black anatase to 90 min.

3.2. Characterization of the black anatase-TiO_2 powder

EPR measurements are shown in Fig. 2(a). This technique is widely used to identify unpaired electrons in paramagnetic materials and confirm the presence of Ti^{3+} species and oxygen vacancies in the samples [65,75–77]. Peaks at $g = 2.001$ [47,48,78] and $g = 2.002$ [79,80] are directly associated with the presence of oxygen vacancies [47,48,78]. However, peak at $g = 2.002$ has been reported to represent an oxygen vacancy combined with one electron [65,81] as well as being ascribed to the Ti^{3+} species [65,82]. Therefore, EPR is a qualitative tool that verifies the existence of oxygen vacancies, but not their concentration. The determination of vacancy concentration is described below.

Fig. 2(b) shows XRD analysis and confirms the anatase crystalline structure of the black TiO_2 powder. XRD pattern is consistent with the standard ICDD card #01–073–1764 (Figure S1) and shows broad peaks at values of $2\theta = 25.40$, 37.07, 37.89, 38.72, 48.12, 54.25 and 55.19°, corresponding to the (101), (004), (200), (105), (204), (116) and (215) reflections [83]. Additionally, the diffraction peaks all exhibit a slight shift towards higher diffraction angles. This indicates a reduced interplanar distance, attributed to the high concentration of oxygen

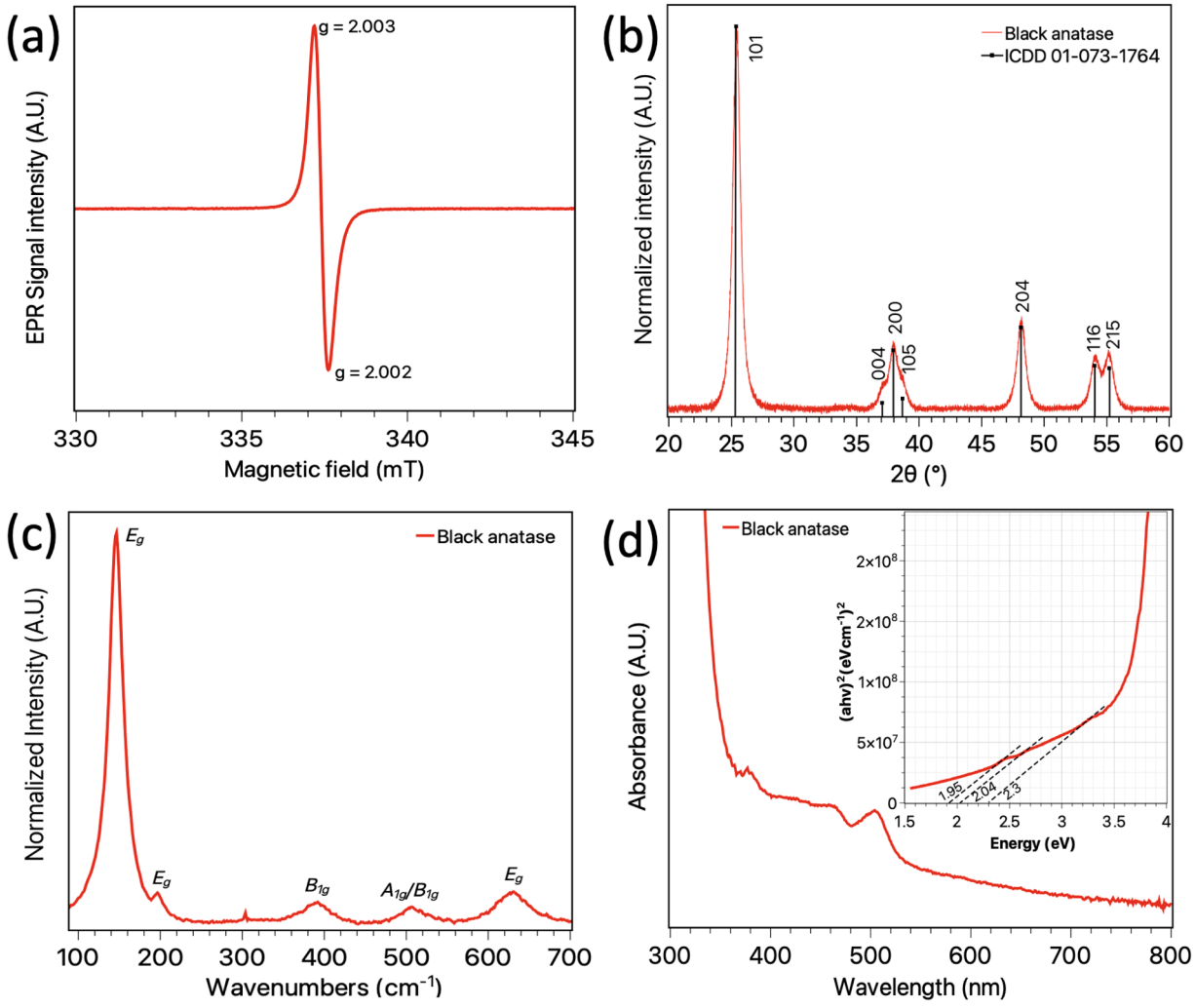

Fig. 2. Characterization of the crystalline structure and optical properties of the black anatase powder. (a) EPR signal; (b) X-ray diffraction scan; (c) Micro-Raman spectroscopy; (d) UV–vis spectra and Tauc plot.

vacancies present in the black anatase [64,84]. Indeed, previous studies have reported a lattice contraction of about 1 to 4 %, induced by the presence of oxygen vacancies in black TiO_2 [23].

Micro-Raman spectroscopy results in Fig. 2(c) also clearly show the characteristics anatase signature with the E_g modes around 146 cm^{-1}, 196 cm^{-1} and 632 cm^{-1} [31,55]. The $A_{1g}/B_{1\ g}$ mode around 507 cm^{-1} and the $B_{1\ g}$ mode around 390 cm^{-1} are also observed. In general, Raman modes can be sensitive to crystal size. For TiO_2, it has been previously shown that grain size has no significant effect on its Raman spectra [85,86]. Here, it was observed that low-wavenumber peaks kept their position at 146 cm^{-1} and 196 cm^{-1}, while the anatase Raman peaks normally at 401, 520 and 643 cm^{-1} [87] shift to slightly lower wavenumbers (390, 506 and 632 cm^{-1} respectively). Similarly to XRD, this can be explained by the high concentrations of oxygen vacancies creating deformations of the lattice producing shifts and broadening of some of its Raman peaks [85]. Oxygen vacancies have been reported to be responsible for the shift and broadening of the anatase E_g Raman modes, which are also sometimes used as a direct indicator for the presence of oxygen vacancies [24,45,86,88–90].

Black anatase UV-visible absorption spectra in Fig. 2(d) shows light absorption bands near 380, 460 and 500 nm, originating from the intra-bandgap energy states created by the oxygen vacancies [64]. Black anatase intra-bandgap energy can be measured directly from the UV-visible absorption spectra by linear extrapolation of the band-edges in the Tauc plot shown in the inset of Fig. 2(d) [91]. There, sub-bandgap absorption starts to occur at photon energies around 1.95, 2.04 and 2.3 eV [92,93].

Chemical composition and ionic states of black anatase were investigated by XPS analysis. C, O and Ti were detected by the survey scan spectra in Fig. 3(a). Ti 2p XPS spectrum and peak area of the black anatase are shown in Fig. 3(b) and summarized in Table S2. Ti 2p3 and Ti 2p1 XPS peaks corresponding to Ti^{3+} of the black anatase are located at 458 and 463 eV, respectively, indicating the existence of surface Ti^{3+} [94]. The concentration of oxygen vacancies was determined as 7.7 % based on the ratio of Ti^{3+} peaks areas [94,95]. This value is consistent with previous oxygen vacancies concentrations reported in literature ranging from 3 % to nearly 8 % [94,95].

Fig. 3(c) shows the O 1 s XPS of the black anatase. The peak at 529 eV is attributed to lattice oxygen; the peak at 531 eV corresponds to the hydroxy oxygen (Ti-OH) or to the alkoxyl radical (Ti-OC) and finally, the peak at 533 eV is ascribed to the uncoordinated oxygen.

TEM is also used to highlight structural properties and morphology of the black anatase powder. As shown in Fig. 4(a), black anatase nanoparticles exhibit an average diameter around 20 nm with lattice fringes visible in Fig. 4(b) and Fig. 4(c). As a result of oxygen vacancies, surface disorder was anticipated [96,97]. The interplanar distance was found to be around 0.35 nm. It is shown in Fig. 4(c) and it confirms the anatase TiO_2 crystalline structure [98].

3.2.1. Black anatase TiO_2 electrode

Immobilization of the photocatalyst on a substrate is a common strategy to improve the photocatalytic process, since this can help with photocatalyst recovery and re-utilization [99]. Photocatalytic reactors with an immobilized photocatalyst generally rely on physical or chemical bonds to fix the catalyst to the support [100]. Previously, such immobilization approaches have yielded 100 % phenol degradation after 4 h under optimal operation conditions [101]. Here, black anatase powder is immobilized atop a glass substrate as detailed in the *Experimental section*. A 4 nm-thick Pt layer is then deposited via sputtering to act as a co-catalyst and maximize photocatalytic degradation [7]. The step-by-step fabrication process and the resulting black anatase TiO_2 electrode after Pt co-catalyst deposition are shown in Fig. 5. Unlike other chemical methods where metallic nanoparticles yield a sparse coating, agglomerates or form clusters [61,97], sputter deposition yields a smooth and uniform coating shown in Fig. 5(b).

The thickness of the co-catalyst Pt layer was tailored to optimize the interaction between the light excitation and the black anatase film. Sputtered Pt films with thicknesses around 13 nm show around 50 % transmission from 400 to 800 nm [102,103]. Based on this, a 4 nm Pt layer was chosen to achieve a trade-off between optical transparency and photocatalytic activity [7].

SEM and EDS elemental mapping are performed to investigate the morphology of the electrode and the distribution of the sputtered platinum co-catalyst. Fig. 6(a) and Fig. 6(b) show the surface in black anatase particles, which range from 2 - 150 μm diameter. Figure S2 illustrates the elemental distribution of the sputtered platinum layer, which closely aligns with the distributions of titanium and oxygen, indicating that the Pt uniformly coats the particles.

3.3. Photocatalytic degradation

The use of black TiO_2 for photocatalytic applications is sometimes controversial due to the presence of Ti^{3+} species among surface defects, which can act as recombination centers and potentially hinder photocatalytic reactions [43]. In the past, this issue was resolved by passivating the Ti^{3+} sites with metallic ions such as Li^+ or Pt [43,104]. In fact, the photocatalytic performance of black TiO_2 can be greatly influenced by a variety of factors, including defect location and concentration, valence and conduction band levels, synthesis route, and synthesis conditions [65]. However, it has been established that these issues are generally related to the synthesis conditions [73]. In contrast, the TiO_2–acetylacetonate synthesis route presented in this study avoids such synthesis conditions and is capable of generating and stabilizing superoxide radicals [72,73,75]. Therefore, the presence of stable free radicals on the surface make this black anatase an active catalyst for the degradation of organic contaminants [72,73].

To test the photocatalytic properties of the platinum-coated black

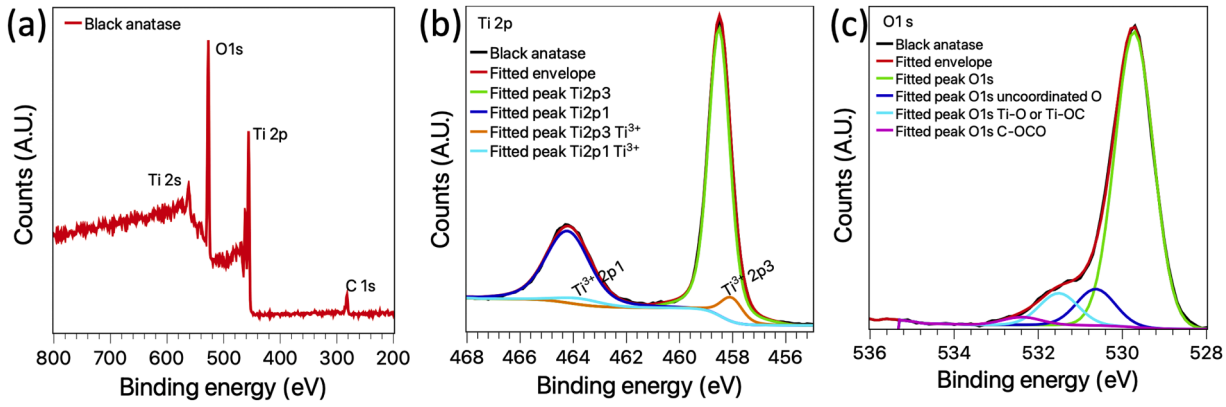

Fig. 3. XPS spectra of the black anatase powder. (a) XPS survey analysis. (b) XPS Ti 2p peaks. (c) XPS O1 s peaks.

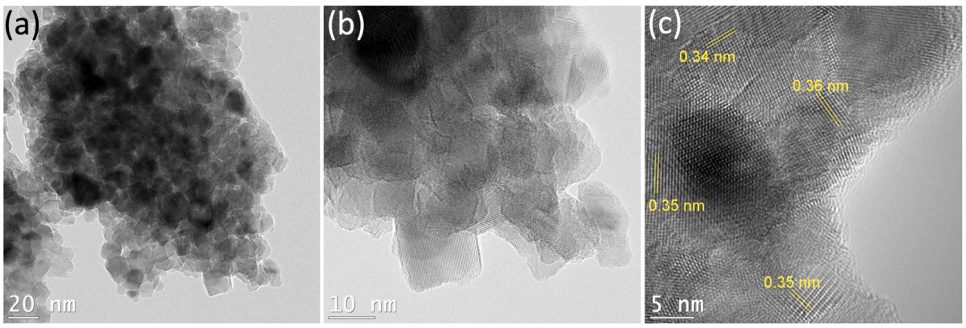

Fig. 4. TEM images of the black anatase TiO_2 powder at different magnifications, with scale bars of (a) 20 nm, (b) 10 nm, (c) 5 nm.

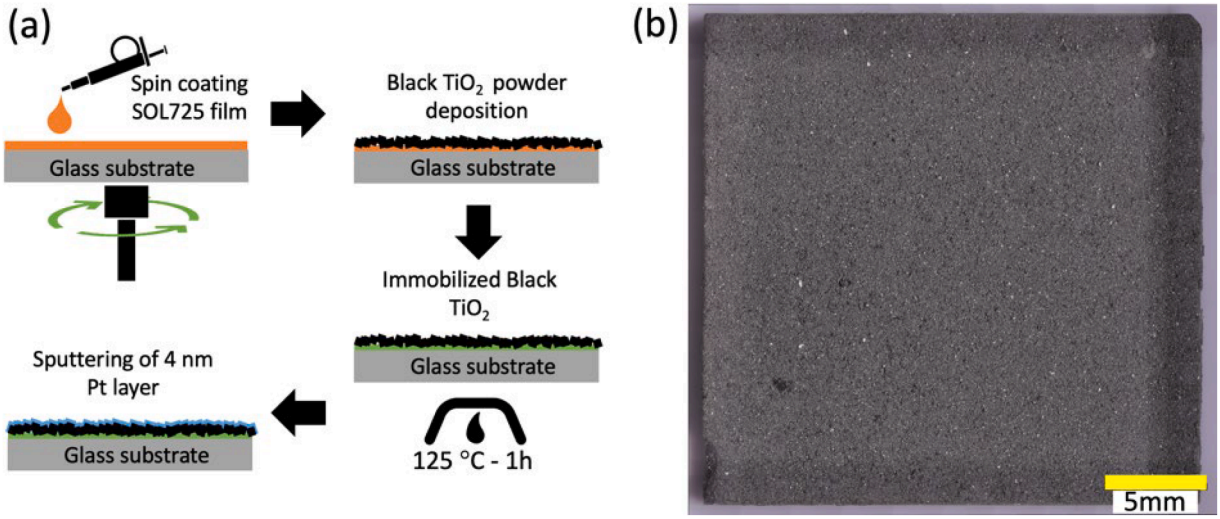

Fig. 5. (a) Schematic representation of the black anatase electrode construction process. (b) Image of the black anatase electrode after Pt sputtering.

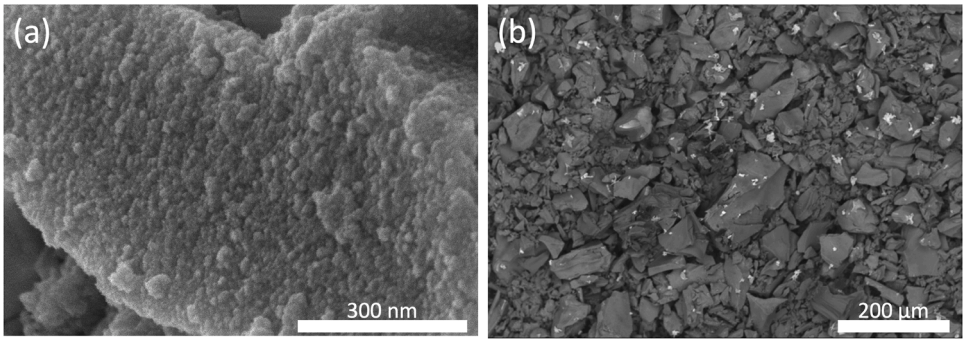

Fig. 6. SEM microscopy of the black anatase electrode at (a) high, (b) low magnification.

anatase electrodes, a 5 mg L^{-1} RhB solution was used as a pollutant model. As the photo-excitation source, a solar simulator (AM 1.5 G) equipped with a long-pass UV filter ($\lambda \geq 400$ nm) was used to ensure that only visible light interacts with the black anatase electrode and to prevent any RhB dye degradation caused by the UV light [105]. Prior the photocatalytic degradation, the black anatase electrode was left in contact with the RhB model solution in the dark for 1 h A negligible adsorption around 5 % was observed (Figure S3). To enhance the reaction, 0.1278 mol of H_2O_2 was also added to the solution. After only 40 min under illumination, Fig. 7(a) shows the electrode yields a 94 % RhB degradation. Thereafter, a second degradation cycle is performed using fresh RhB solution with the same electrode. The degradation remains at 89 % after 65 min. As a control experiment, a similar electrode using immobilized powder of commercial Degussa P25 TiO_2, which does not possess oxygen vacancies, was prepared and tested under the same experimental conditions. As shown in Fig. 7(a), the photocatalytic RhB degradation using Degussa P25 is negligible, since it can only be activated under UV-light [106]. The limited degradation observed with Degussa P25 can be attributed to nitrogen de-ethylation of the RhB, which occurs under visible light through a photo-induced electron transfer between the adsorbed dye and the Degussa P25, without the participation of reactive oxygen species [107]. Therefore, it can be concluded that oxygen vacancies from the black TiO_2 powder (i) are absorbing light and (ii) are responsible for the degradation of RhB.

Spectral evolution of the RhB absorption curve during the photocatalytic degradation measured at 5-minute intervals is displayed in

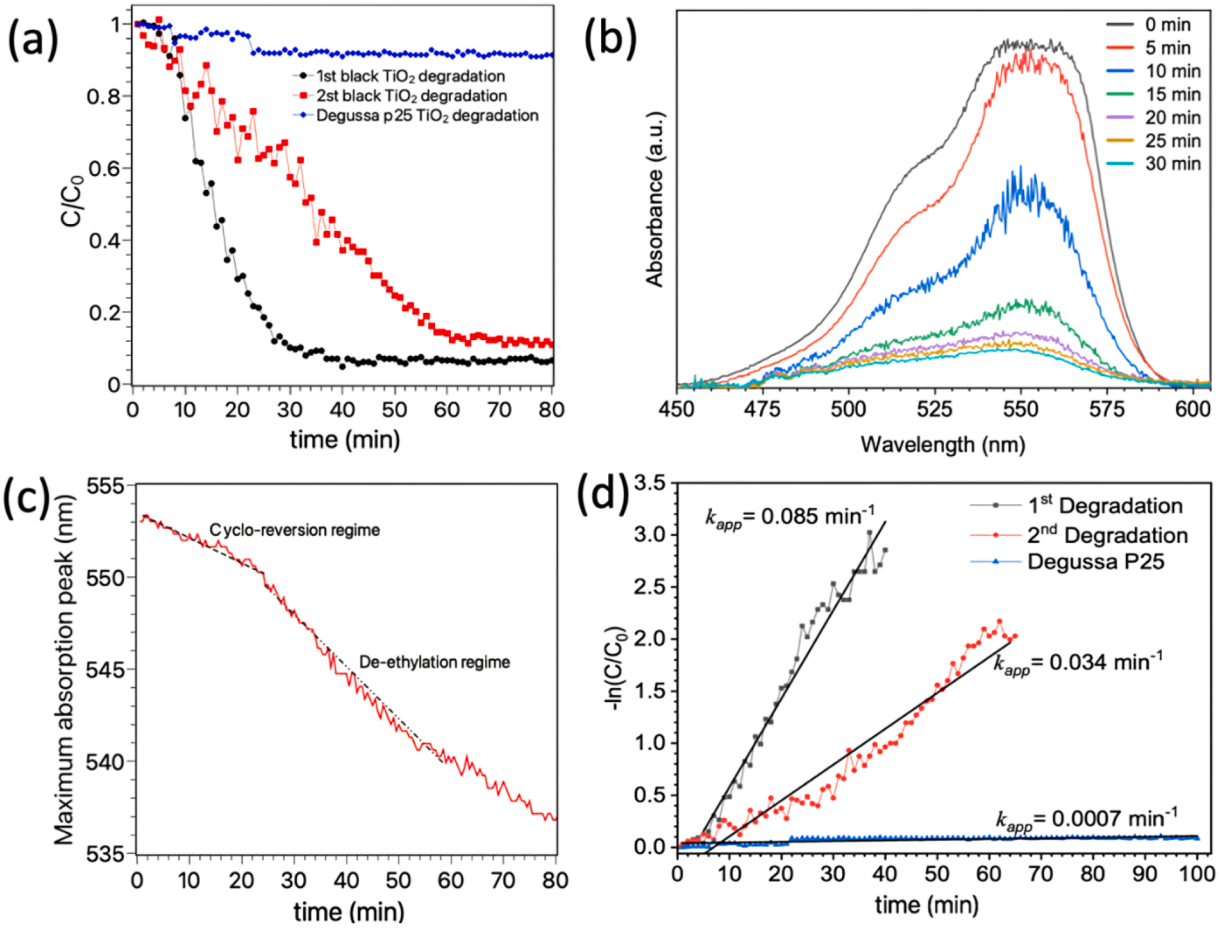

Fig. 7. Photocatalytic degradation of RhB. (a) Efficiency of the first and second cycles of photocatalytic degradation of RhB using the black anatase electrode, compared with the performance of commercial Degussa P25 TiO_2. (b) Spectral evolution of the RhB absorbance during the photocatalytic degradation reaction. (c) Evolution of the absorption peak position evolution during the photocatalytic degradation. The two dashed lines indicate the two distinct regimes occurring during the degradation. (d) Pseudo-first-order kinetics fitting plots for the first and the second RhB degradation. Fitting plot for the Degussa P25 RhB degradation.

Fig. 7(b). As expected, RhB absorbance decreases as the photocatalytic degradation reaction evolves. Most importantly, Fig. 7(c) shows two degradation regimes and a clear blue-shift in the RhB absorption peak as soon as the photodegradation reaction is triggered. Nearly 80 % of the RhB degradation occurs in the initial 20 min of the cycle. Meanwhile, the absorbance shows only a very modest blue shift, going from 553 nm to 550 nm. This is because the RhB decomposition is initially achieved by the cleavage of the whole chromophore structure (i.e. cycloreversion) [108]. After 20 min, the absorption peak rapidly shifts from 550 nm down to 537 nm. According to the literature, the peak absorption of the N,N,N'-Triethyl-rhodamine by-product resulting from the cleavage is located at 539 nm [109]. This suggests that the de-ethylation dominates the photocatalytic degradation after the first 20 min [7,109,110]. For the second degradation cycle shown in Fig. 7(a), the RhB degradation efficiency drops slightly from 94 % to 89 %. This reduction is most likely due to the partial destruction or saturation of the photocatalytic sites [7]. Previous reports show that RhB can be adsorbed on the TiO_2 surface through the negatively-charged carboxyl group [111].

To examine more accurately the photocatalytic performance, a comparative analysis was done on the reaction kinetics for the first and second RhB degradations under visible-light irradiation against the kinetics of Degussa P25. The assessment of photocatalytic activity was quantitatively determined through the calculation of apparent reaction rate constants k_{app}. The kinetics fitting plots of the first, second and Degusa P25 RhB degradations are shown in Fig. 7(d). The degradation curves were fitted using the pseudo-first-order kinetic equation, $-\ln(C/C_0) = k_{app}\, t$, which yielded R-square values above 0.96, indicating a high level of correlation. In this equation, C denotes the concentration of RhB at time t, C_0 signifies the initial concentration of RhB, k_{app} is the first-order apparent kinetic constant (min^{-1}), and t represents the elapsed time [112]. It was observed that the rate constants k_{app} for both the first and second degradations follow to the Langmuir–Hinshelwood model [113], whereas the k_{app} for the Degussa P25 degradation is close to cero since it exhibited a negligible degradation. The reaction rate constants k_{app}, the photocatalytic degradation rate and the R^2 values for the first, second and the Degussa P25 degradation are summarized in the Table 1.

As anticipated, these remarkable photocatalytic efficiencies under visible light can be directly attributed to the presence of oxygen vacancies [65,72,73], which enhance performance by generating active trapping centers that reduce the recombination of photo-generated carriers and extend the light response range through intraband gap energy levels below the conduction band of black anatase [30,92,94].

Table 1
Photocatalytic properties of black anatase TiO_2 and Degussa P25 under visible-light irradiation.

Sample	RhB photocatalytic degradation rate (%)	Reaction rate constant, k_{app} (min^{-1})	R^2
Back anatase TiO_2 1st degradation	94	0.085	0.97
Back anatase TiO_2 2nd degradation	89	0.034	0.96
Degussa P25	8	0.0007	0.99

Moreover, the Schottky barrier formed between the Pt and black anatase further improves the extraction of the photogenerated charge carriers [114], resulting in even more efficient RhB degradation [7].

3.3.1. Scavenging process

H_2O_2 interacts with the Pt co-catalyst, acting as a reducing agent yielding hydroxyl groups, or as an oxidizing agent forming O_2 molecules depending on the Pt surface states [115]. In both cases, the H_2O_2 degradation generates highly reactive species with a short lifetime, which are known to govern the photocatalytic reactions [116,117] and to react actively with cationic dyes, such as RhB [118]. The role of Pt in the formation of free radical species and their participation in the photocatalytic degradation of RhB can be indirectly elucidated using four different types of scavengers [119]. Silver nitrate ($AgNO_3$, an electron scavenger), benzoquinone (BQ, a superoxide radical scavenger), triethanolamine (EDTA, a hole scavenger) and tert-butanol (TBA, a hydroxyl radical scavenger) were explored, and their influence over the photocatalytic degradation is summarized in Fig. 8(a).

All these scavengers significantly impede the RhB photocatalytic degradation. AgNO3, an electron scavenger, significantly hampers the degradation reaction, decreasing its degradation rate from 94 % to only 6 %. Similarly, a superoxide radical scavenger (BQ) brings the degradation rate to about 17 %. Furthermore, the degradation reaction rate falls to 33 % when using the hydroxyl radical scavenger (TBA), and 35 % for the hole scavenger (EDTA). It is evident that photo-generated electrons, along with superoxide radicals, are the predominant species involved in the RhB degradation reaction [118,120]. Black anatase-TiO_2 is an n-type material [121] meaning it has an abundance of free electrons available for conduction. When coupled with a thin Pt layer, which acts as an electron sink, the Pt efficiently captures and traps the electrons generated in TiO_2 during the photocatalytic process. This electron trapping reduces the likelihood of electron-hole recombination, allowing more electrons to participate in the desired photocatalytic reactions, thereby enhancing the overall efficiency of the process [7]. Fig. 8(b) depicts the proposed photocatalytic mechanism performed under visible light.

The proposed photocatalytic system offers several advancements over conventional nanoparticle-based methods. Notably, the integration of an oxygen vacancy-rich photocatalyst with a Pt co-catalyst enhances the degradation rates under visible light, a significant improvement given that many state-of-the-art photocatalysts require UV light to achieve optimal activity. Furthermore, the immobilization of photocatalyst nanoparticles addresses the common issue of turbidity affecting degradation rates, presenting a clear advantage in terms of process efficiency and cost-effectiveness. By eliminating the need for photocatalyst recovery, this methodology simplifies the treatment process, reducing both operational complexity and expense, which are critical considerations in large-scale applications [122]. The proposed methodology demonstrates a balance of environmental friendliness, operational simplicity, and cost-efficiency.

4. Conclusion

This work presents a cost-effective method to crystallize black anatase in air and ambient conditions, avoiding the requirements of long duration, high temperature, vacuum or high-pressure synthesis processes used in prior works. We also report the use of black anatase as a highly efficient, sunlight-activated photocatalyst technology using only visible light. In-situ monitoring of the degradation of RhB, a pollutant model, is demonstrated using absorption measurements, and the highly reactive features of different scavengers are used to study the degradation mechanisms of RhB. This study demonstrates that photo-generated electrons and superoxide radicals play a significant role in the photocatalytic degradation process, which results in an impressive 94 % reduction of Rhodamine B within a brief period upon exposure to visible sunlight. These performance characteristics are explained by (i) long-term stability and high-performance of the black anatase, (ii) the presence of oxygen vacancies that enable the visible light response of the black anatase while reducing the recombination of photo-generated carriers, and (iii) the effective Schottky barrier introduced using a 4 nm-thick platinum coating of the electrode to act as a co-catalyst. Compared to state-of-the art Degussa P25 TiO_2, black anatase as a supported photocatalyst achieves highly efficient pollutant degradation under visible light only. These results pave the way for commercially attractive technologies to treat polluted water using visible light, bringing highly efficient photocatalysis processes closer to large-scale deployment. While this study presents significant advancements in photocatalyst technology, it is important to consider potential limitations. The scalability of the black anatase crystallization process under ambient conditions for industrial applications has not been yet addressed. Furthermore, the long-term environmental impact of black anatase remain to be fully assessed. Additionally, the comparative analysis with Degussa P25 TiO_2 does not account for the full spectrum of photocatalytic materials available, which may offer different benefits. Lastly, the economic feasibility of large-scale implementation of this technology, considering the cost of platinum and the overall system design, requires further investigation.

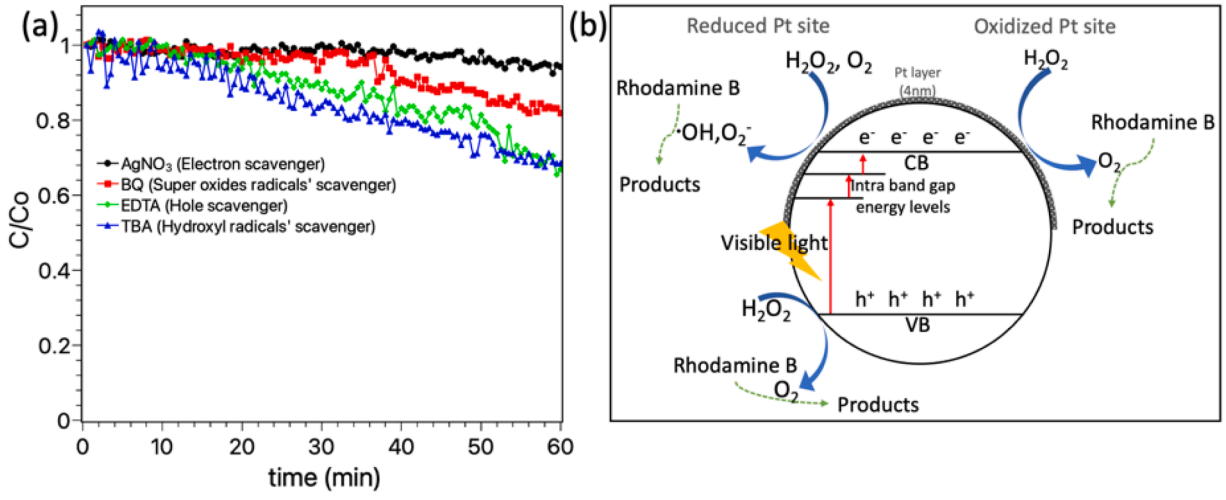

Fig. 8. (a) Influence of different scavengers on the photocatalytic degradation of RhB. (b) Schematic representation of the photocatalytic RhB degradation mechanisms under visible light illumination.

Supporting Information

Supporting Information is available upon request.

CRediT authorship contribution statement

Jaime A. Benavides-Guerrero: Writing – original draft, Visualization, Validation, Software, Project administration, Methodology, Investigation, Formal analysis, Data curation, Conceptualization. **Paul Fourmont:** Writing – review & editing, Validation, Software, Methodology, Investigation, Formal analysis, Data curation. **Luis Felipe Gerlein:** Writing – review & editing, Validation, Software, Resources, Methodology, Formal analysis, Data curation. **Astrid C. Angel-Ospina:** Software, Methodology, Investigation. **Fiderman Machuca-Martinez:** Writing – review & editing, Software, Resources, Formal analysis. **Fabrice Vaussenat:** Writing – review & editing, Visualization, Software, Resources, Methodology. **Caroline A. Ross:** Writing – review & editing, Validation, Supervision, Project administration, Methodology, Investigation, Formal analysis, Data curation. **Sylvain G. Cloutier:** Writing – review & editing, Validation, Supervision, Resources, Project administration, Investigation, Funding acquisition, Formal analysis, Data curation.

Declaration of competing interest

The authors declare that they have no known competing financial interests or personal relationships that could have appeared to influence the work reported in this paper.

Acknowledgement

Sylvain G. Cloutier thanks the Canada Research Chair and the NSERC Discovery pro- grams for their support.

Supplementary materials

Supplementary material associated with this article can be found, in the online version, at doi:10.1016/j.surfin.2025.105849.

Data availability

Data will be made available on request.

References

[1] K.R. Davies, B. Jones, C. Terashima, A. Fujishima, S. Pitchaimuthu, Photocatalytic water pollutant treatment: fundamental, analysis and benchmarking, in: S. Balakumar, V. Keller, M.V. Shankar (Eds.), Nanostructured Materials for Environmental Applications, Springer International Publishing, Cham, 2021, pp. 401–431, https://doi.org/10.1007/978-3-030-72076-6_16.
[2] A. Fujishima, K. Honda, Electrochemical photolysis of water at a semiconductor electrode, Nature 238 (1972) 37–38, https://doi.org/10.1038/238037a0.
[3] S.N. Frank, A.J. Bard, Heterogeneous photocatalytic oxidation of cyanide and sulfite in aqueous solutions at semiconductor powders, J. Phys. Chem. 81 (1977) 1484–1488, https://doi.org/10.1021/j100530a011.
[4] A.A. Belhekar, S.V. Awate, R. Anand, Photocatalytic activity of titania modified mesoporous silica for pollution control, Catal. Commun. 3 (2002) 453–458, https://doi.org/10.1016/S1566-7367(02)00179-6.
[5] S. Zhu, D. Wang, Photocatalysis: basic principles, diverse forms of implementations and emerging scientific opportunities, Adv. Energy Mater. 7 (2017) 1700841, https://doi.org/10.1002/aenm.201700841.
[6] R. Li, T. Li, Q. Zhou, Impact of titanium dioxide (TiO2) modification on its application to pollution treatment—a review, Catalysts. 10 (2020) 804, https://doi.org/10.3390/catal10070804.
[7] P. Fourmont, R. Nechache, S.G. Cloutier, Reusable BiFeO3 nanofiber-based membranes for photo-activated organic pollutant removal with negligible colloidal release, ACS Appl. Nano Mater. 4 (2021) 12261–12269, https://doi.org/10.1021/acsanm.1c02762.
[8] R. Saravanan, F. Gracia, A. Stephen, Basic Principles, Mechanism, and Challenges of Photocatalysis, in: M.M. Khan, D. Pradhan, Y. Sohn (Eds.), Nanocomposites For Visible Light-Induced Photocatalysis, 1st ed., Springer International Publishing, Cham, 2017, pp. 19–40, https://doi.org/10.1007/978-3-319-62446-4_2.
[9] M.A. Fox, M.T. Dulay, Heterogeneous photocatalysis, Chem. Rev. (United States) 93 (1993) 341–357, https://doi.org/10.1021/cr00017a016.
[10] M. Mishra, D.-M. Chun, α-Fe2O3 as a photocatalytic material: a review, Appl. Catal. A: General 498 (2015) 126–141, https://doi.org/10.1016/j.apcata.2015.03.023.
[11] Z. Zhao, X. Zhang, Y. Lei, P. Yang, J. Fan, B. Zhang, S. Yin, Exceptional photocatalytic activity for Ag,Cr- SrTiO3 activated by H2O2 for removal of organic pollutants, Mater. Res. Express 7 (2020) 015034, https://doi.org/10.1088/2053-1591/ab6246.
[12] R. Georgekutty, M.K. Seery, S.C. Pillai, A Highly Efficient Ag-ZnO photocatalyst: synthesis, properties, and mechanism, J. Phys. Chem. C 112 (2008) 13563–13570, https://doi.org/10.1021/jp802729a.
[13] W. Zeng, T. Cai, Y. Liu, L. Wang, W. Dong, H. Chen, X. Xia, An artificial organic-inorganic Z-scheme photocatalyst WO3@Cu@PDI supramolecular with excellent visible light absorption and photocatalytic activity, Chem.Eng. J. 381 (2020) 122691, https://doi.org/10.1016/j.cej.2019.122691.
[14] Q. Wang, K. Edalati, Y. Koganemaru, S. Nakamura, M. Watanabe, T. Ishihara, Z. Horita, Photocatalytic hydrogen generation on low-bandgap black zirconia (ZrO 2) produced by high-pressure torsion, J. Mater. Chem. A 8 (2020) 3643–3650, https://doi.org/10.1039/C9TA11839J.
[15] P. Fourmont, S.G. Cloutier, Screen-printed p–n BiOCl/BiFeO 3 heterojunctions for efficient photocatalytic degradation of Rhodamine B, RSC. Adv. 12 (2022) 24868–24875, https://doi.org/10.1039/D2RA03308A.
[16] K. Nakata, A. Fujishima, TiO2 photocatalysis: design and applications, J. Photochem. Photobiol. C 13 (2012) 169–189, https://doi.org/10.1016/j.jphotochemrev.2012.06.001.
[17] R.N. Araujo, E.P. Nascimento, H.C.T. Firmino, D.A. Macedo, G.A. Neves, M. A. Morales, R.R. Menezes, α-Fe2O3 fibers: an efficient photocatalyst for dye degradation under visible light, J. Alloys. Compd. 882 (2021) 160683, https://doi.org/10.1016/j.jallcom.2021.160683.
[18] T. Xian, H. Yang, L. Di, J. Ma, H. Zhang, J. Dai, Photocatalytic reduction synthesis of SrTiO3-graphene nanocomposites and their enhanced photocatalytic activity, Nanoscale Res. Lett. 9 (2014) 327, https://doi.org/10.1186/1556-276X-9-327.
[19] C. Karthikeyan, P. Arunachalam, K. Ramachandran, A.M. Al-Mayouf, S. Karuppuchamy, Recent advances in semiconductor metal oxides with enhanced methods for solar photocatalytic applications, J. Alloys. Compd. 828 (2020) 154281, https://doi.org/10.1016/j.jallcom.2020.154281.
[20] M.B. Tahir, G. Nabi, A. Hassan, T. Iqbal, H. Kiran, A. Majid, Morphology tailored synthesis of C-WO3 nanostructures and its photocatalytic application, J. Inorg. Organomet. Polym. 28 (2018) 738–745, https://doi.org/10.1007/s10904-017-0720-8.
[21] M. Mansouri, N. Mozafari, B. Bayati, N. Setareshenas, Photo-catalytic dye degradation of methyl orange using zirconia–zeolite nanoparticles, Bull. Mater. Sci 42 (2019) 230, https://doi.org/10.1007/s12034-019-1933-y.
[22] K.E. O'Shea, E. Pernas, J. Saiers, The influence of mineralization products on the coagulation of TiO2 photocatalyst, Langmuir 15 (1999) 2071–2076, https://doi.org/10.1021/la9806808.
[23] A. Naldoni, M. Allieta, S. Santangelo, M. Marelli, F. Fabbri, S. Cappelli, C. L. Bianchi, R. Psaro, V. Dal Santo, Effect of nature and location of defects on bandgap narrowing in black TiO2 nanoparticles, J. Am. Chem. Soc. 134 (2012) 7600–7603, https://doi.org/10.1021/ja3012676.
[24] B. Choudhury, A. Choudhury, Oxygen defect dependent variation of band gap, Urbach energy and luminescence property of anatase, anatase–rutile mixed phase and of rutile phases of TiO2 nanoparticles, Physica E 56 (2014) 364–371, https://doi.org/10.1016/j.physe.2013.10.014.
[25] M. Umar, H.A. Aziz, Photocatalytic degradation of organic pollutants in water, IntechOpen (2013), https://doi.org/10.5772/53699.
[26] J. You, Y. Guo, R. Guo, X. Liu, A review of visible light-active photocatalysts for water disinfection: features and prospects, Chem. Eng. J. 373 (2019) 624–641, https://doi.org/10.1016/j.cej.2019.05.071.
[27] K. Kabra, R. Chaudhary, R.L. Sawhney, Treatment of hazardous organic and inorganic compounds through aqueous-phase photocatalysis: a review, Ind. Eng. Chem. Res. 43 (2004) 7683–7696, https://doi.org/10.1021/ie0498551.
[28] E. Roduner, Size matters: why nanomaterials are different, Chem. Soc. Rev. 35 (2006) 583–592, https://doi.org/10.1039/B502142C.
[29] J. Tian, Z. Zhao, A. Kumar, R.I. Boughton, H. Liu, Recent progress in design, synthesis, and applications of one-dimensional TiO 2 nanostructured surface heterostructures: a review, Chem. Soc. Rev. 43 (2014) 6920–6937, https://doi.org/10.1039/C4CS00180J.
[30] X. Xin, T. Xu, J. Yin, L. Wang, C. Wang, Management on the location and concentration of Ti3+ in anatase TiO2 for defects-induced visible-light photocatalysis, Appl. Catal. B 176–177 (2015) 354–362, https://doi.org/10.1016/j.apcatb.2015.04.016.
[31] J.A. Benavides, C.P. Trudeau, L.F. Gerlein, S.G. Cloutier, Laser selective photoactivation of amorphous TiO2 films to anatase and/or rutile crystalline phases, ACS Appl. Energy Mater. 1 (2018) 3607–3613, https://doi.org/10.1021/acsaem.8b00171.
[32] M. Manzoli, F.S. Freyria, N. Blangetti, B. Bonelli, Brookite, a sometimes under evaluated TiO2 polymorph, RSC. Adv. 12 (2022) 3322–3334, https://doi.org/10.1039/D1RA09057G.
[33] H. de Lasa, B. Serrano, M. Salaices, Photocatalytic Reaction Engineering, 1st ed, Springer Science & Business Media, 2005, https://doi.org/10.1007/0-387-27591-6.
[34] H. Deng, H. He, S. Sun, X. Zhu, D. Zhou, F. Han, B. Huang, X. Pan, Photocatalytic degradation of dye by Ag/TiO2 nanoparticles prepared with different sol–gel

crystallization in the presence of effluent organic matter, Environ. Sci. Pollut. Res. 26 (2019) 35900–35912, https://doi.org/10.1007/s11356-019-06728-0.
[35] T. Yoshida, Y. Misu, M. Yamamoto, T. Tanabe, J. Kumagai, S. Ogawa, S. Yagi, Effects of the amount of Au nanoparticles on the visible light response of TiO2 photocatalysts, Catal. Today 352 (2020) 34–38, https://doi.org/10.1016/j.cattod.2019.12.035.
[36] L. Yang, Z. Chen, J. Zhang, C.-A. Wang, SrTiO3/TiO2 heterostructure nanowires with enhanced electron-hole separation for efficient photocatalytic activity, Front. Mater. Sci. 13 (2019) 342–351, https://doi.org/10.1007/s11706-019-0477-9.
[37] L. Zhao, Y. Xie, Q. Lin, R. Zheng, Y. Diao, Preparation of C, N and P co-doped TiO2 and its photocatalytic activity under visible light, Funct. Mater. Lett. 12 (2019) 1950045, https://doi.org/10.1142/S1793604719500450.
[38] L. Hlekelele, S.H. Durbach, V.P. Chauke, F. Dziike, P.J. Franklyn, Resin-gel incorporation of high concentrations of W6+ and Zn2+ into TiO2-anatase crystal to form quaternary mixed-metal oxides: effect on the a lattice parameter and photodegradation efficiency, RSC. Adv. 9 (2019) 36875–36883, https://doi.org/10.1039/C9RA07355H.
[39] X. Lai, Light manipulation in a dually ordered porous TiO 2 –rGO composite for efficient solar energy utilization, Inorg. Chem. Front. 4 (2017) 578–580, https://doi.org/10.1039/C7QI00053G.
[40] W. Jiao, L. Zhang, R. Yang, J. Ning, L. Xiao, Y. Liu, J. Ma, N. Mahmood, X. Jian, Synthesis of monolayer carbon-coated TiO2 as visible-light-responsive photocatalysts, Appl. Mater. Today 27 (2022) 101498, https://doi.org/10.1016/j.apmt.2022.101498.
[41] F. Zuo, L. Wang, T. Wu, Z. Zhang, D. Borchardt, P. Feng, Self-doped Ti3+ enhanced photocatalyst for hydrogen production under visible light, J. Am. Chem. Soc. 132 (2010) 11856–11857, https://doi.org/10.1021/ja103843d.
[42] I. Justicia, P. Ordejón, G. Canto, J. l. Mozos, J. Fraxedas, G. a. Battiston, R. Gerbasi, A. Figueras, Designed self-doped titanium oxide thin films for efficient visible-light photocatalysis, Adv. Mater. 14 (2002) 1399–1402, https://doi.org/10.1002/1521-4095(20021002)14:19<1399::AID−ADMA1399>3.0.CO;2-C.
[43] Á. Balog, G.F. Samu, S. Pető, C. Janáky, The Mystery of black TiO2: insights from combined surface science and in situ electrochemical methods, ACS Mater. Au 1 (2021) 157–168, https://doi.org/10.1021/acsmaterialsau.1c00020.
[44] Y. Yang, L.-C. Yin, Y. Gong, P. Niu, J.-Q. Wang, L. Gu, X. Chen, G. Liu, L. Wang, H.-M. Cheng, An unusual strong visible-light absorption band in red anatase TiO2 photocatalyst induced by atomic hydrogen-occupied oxygen vacancies, Adv. Mater. 30 (2018) 1704479, https://doi.org/10.1002/adma.201704479.
[45] J.A. Benavides-Guerrero, L.F. Gerlein, C. Trudeau, D. Banerjee, X. Guo, S. G. Cloutier, Synthesis of vacancy-rich titania particles suitable for the additive manufacturing of ceramics, Sci. Rep. 12 (2022) 15441, https://doi.org/10.1038/s41598-022-19824-y.
[46] X. Chen, L. Liu, F. Huang, Black titanium dioxide (TiO2) nanomaterials, Chem. Soc. Rev. 44 (2015) 1861–1885, https://doi.org/10.1039/C4CS00330F.
[47] R. Katal, M. Salehi, M.H. Davood Abadi Farahani, S. Masudy-Panah, S.L. Ong, J. Hu, Preparation of a new type of black TiO2 under a vacuum atmosphere for sunlight photocatalysis, ACS Appl. Mater. Interfaces 10 (2018) 35316–35326, https://doi.org/10.1021/acsami.8b14680.
[48] C.-C. Wang, P.-H. Chou, Effects of various hydrogenated treatments on formation and photocatalytic activity of black TiO2 nanowire arrays, Nanotechnology. 27 (2016) 325401, https://doi.org/10.1088/0957-4484/27/32/325401.
[49] S. Sun, H. Yu, L. Li, X. Yu, X. Zhang, Z. Lu, X. Yang, Sodium borohydride treatment to prepare manganese oxides with oxygen vacancy defects for efficient oxygen reduction, Metals. (Basel) 12 (2022) 1059, https://doi.org/10.3390/met12071059.
[50] W. Fang, M. Xing, J. Zhang, Modifications on reduced titanium dioxide photocatalysts: a review, J. Photochem. Photobiol. C 32 (2017) 21–39, https://doi.org/10.1016/j.jphotochemrev.2017.05.003.
[51] N. Liu, C. Schneider, D. Freitag, U. Venkatesan, V.R.R. Marthala, M. Hartmann, B. Winter, E. Spiecker, A. Osvet, E.M. Zolnhofer, K. Meyer, T. Nakajima, X. Zhou, P. Schmuki, Hydrogenated anatase: strong photocatalytic dihydrogen evolution without the use of a co-catalyst, Angewandte Chemie Int. Ed. 53 (2014) 14201–14205, https://doi.org/10.1002/anie.201408493.
[52] U. Diebold, The surface science of titanium dioxide, Surf. Sci. Rep. 48 (2003) 53–229, https://doi.org/10.1016/S0167-5729(02)00100-0.
[53] A. Sarkar, G. Gopal Khan, The formation and detection techniques of oxygen vacancies in titanium oxide-based nanostructures, Nanoscale 11 (2019) 3414–3444, https://doi.org/10.1039/C8NR09666J.
[54] X. Pan, M.-Q. Yang, X. Fu, N. Zhang, Y.-J. Xu, Defective TiO2 with oxygen vacancies: synthesis, properties and photocatalytic applications, Nanoscale 5 (2013) 3601–3614, https://doi.org/10.1039/C3NR00476G.
[55] L.F. Gerlein, J.A. Benavides-Guerrero, S.G. Cloutier, Laser-assisted, large-area selective crystallization and patterning of titanium dioxide polymorphs, Adv. Eng. Mater. 22 (2020) 1901014, https://doi.org/10.1002/adem.201901014.
[56] R. Schaub, E. Wahlstrom, A. Rennau, E. Laegsgaard, et al., Oxygen-mediated diffusion of oxygen vacancies on the TiO2(110) surface, Science (1979) 299 (2003) 377–379, https://doi.org/10.1126/science.107896.
[57] M. Setvín, U. Aschauer, P. Scheiber, L. Ye-Fei, W. Hou, M. Schmid, A. Selloni, U. Diebold, Reaction of O2 with subsurface oxygen vacancies on TiO2 anatase (101), Science (1979) 341 (2013) 988–991, https://doi.org/10.1126/science.1239879.
[58] L. Liu, X. Chen, Titanium dioxide nanomaterials: self-structural modifications, Chem. Rev 114 (2014) 9890–9918, https://doi.org/10.1021/cr400624r.
[59] N. Serpone, Is the Band Gap of Pristine TiO2 Narrowed by Anion- and Cation-Doping of Titanium Dioxide in Second-Generation Photocatalysts? J. Phys. Chem. B 110 (2006) 24287–24293, https://doi.org/10.1021/jp065659r.
[60] W.H. Saputera, J. Scott, N. Ganda, G.K.-C. Low, R. Amal, The role of adsorbed oxygen in formic acid oxidation by Pt/TiO 2 facilitated by light pre-treatment, Catal. Sci. Technol. 6 (2016) 6679–6687, https://doi.org/10.1039/C6CY00939E.
[61] X. Pan, Y.-J. Xu, Defect-mediated growth of noble-metal (Ag, Pt, and Pd) nanoparticles on TiO2 with oxygen vacancies for photocatalytic redox reactions under visible light, J. Phys. Chem. C 117 (2013) 17996–18005, https://doi.org/10.1021/jp4064802.
[62] Y. Han, C. Liu, Q. Ge, Effect of surface oxygen vacancy on Pt cluster adsorption and growth on the defective anatase TiO2(101) surface, J. Phys. Chem. C 111 (2007) 16397–16404, https://doi.org/10.1021/jp075602k.
[63] X. Chen, L. Liu, P.Y. Yu, S.S. Mao, Increasing solar absorption for photocatalysis with black hydrogenated titanium dioxide nanocrystals, Science (1979) 331 (2011) 746–750, https://doi.org/10.1126/science.1200448.
[64] S. Chen, Y. Xiao, Y. Wang, Z. Hu, H. Zhao, W. Xie, A facile approach to prepare black TiO2 with oxygen vacancy for enhancing photocatalytic activity, Nanomaterials 8 (2018) 245, https://doi.org/10.3390/nano8040245.
[65] T.S. Rajaraman, S.P. Parikh, V.G. Gandhi, Black TiO2: a review of its properties and conflicting trends, Chem. Eng. J. 389 (2020) 123918, https://doi.org/10.1016/j.cej.2019.123918.
[66] R. Jonathan, S.U. Rehman, F. Cao, H. Xu, X. Ma, J. Wang, Y. Liu, Y. Niu, X. Jian, N. Mahmood, Low-cost and large-scale preparation of ultrafine TiO2@C hybrids for high-performance degradation of methyl orange and formaldehyde under visible light, Nanotechnol. Rev. 12 (2023), https://doi.org/10.1515/ntrev-2022-0556.
[67] H. Zangeneh, A.A.L. Zinatizadeh, M. Habibi, M. Akia, M. Hasnain Isa, Photocatalytic oxidation of organic dyes and pollutants in wastewater using different modified titanium dioxides: a comparative review, J. Ind. Eng. Chem. 26 (2015) 1–36, https://doi.org/10.1016/j.jiec.2014.10.043.
[68] A.Y. Shan, T.I.Mohd. Ghazi, S.A. Rashid, Immobilisation of titanium dioxide onto supporting materials in heterogeneous photocatalysis: a review, Appl. Catal. A: General 389 (2010) 1–8, https://doi.org/10.1016/j.apcata.2010.08.053.
[69] A.C. Pierre, The chemistry of precursors solutions. Introduction to Sol-Gel Processing, Springer, Boston, MA, 1998, pp. 11–89, https://doi.org/10.1007/978-1-4615-5659-6_2.
[70] D. Hoebbel, T. Reinert, H. Schmidt, E. Arpac, On the hydrolytic stability of organic ligands in Al-, Ti- and Zr-alkoxide complexes, J. Solgel. Sci. Technol. 10 (1997) 115–126, https://doi.org/10.1023/A:1018305811088.
[71] U. Schubert, Organically modified transition metal alkoxides: chemical problems and structural issues on the way to materials syntheses, Acc. Chem. Res. 40 (2007) 730–737, https://doi.org/10.1021/ar600036x.
[72] F. Sannino, P. Pernice, C. Imparato, A. Aronne, G. D'Errico, L. Minieri, M. Perfetti, D. Pirozzi, Hybrid TiO2–acetylacetonate amorphous gel-derived material with stably adsorbed superoxide radical active in oxidative degradation of organic pollutants, RSC. Adv. 5 (2015) 93831–93839, https://doi.org/10.1039/C5RA21176J.
[73] A. Aronne, M. Fantauzzi, C. Imparato, D. Atzei, L.D. Stefano, G. D'Errico, F. Sannino, I. Rea, D. Pirozzi, B. Elsener, P. Pernice, A. Rossi, Electronic properties of TiO2-based materials characterized by high Ti3+ self-doping and low recombination rate of electron–hole pairs, RSC. Adv. 7 (2017) 2373–2381, https://doi.org/10.1039/C6RA27111A.
[74] J. Livage, Synthesis, structure and applications of TiO2 Gels, MRS Online Proceedings Library Archive 72 (1986), https://doi.org/10.1557/PROC-72-323.
[75] C. Imparato, M. Fantauzzi, C. Passiu, I. Rea, C. Ricca, U. Aschauer, F. Sannino, G. D'Errico, L. De Stefano, A. Rossi, A. Aronne, Unraveling the charge state of oxygen vacancies in ZrO2–x on the basis of synergistic computational and experimental evidence, J. Phys. Chem. C 123 (2019) 11581–11590, https://doi.org/10.1021/acs.jpcc.9b00411.
[76] Z. Li, S. Wang, J. Wu, W. Zhou, Recent progress in defective TiO2 photocatalysts for energy and environmental applications, Renewable Sustainable Energy Rev. 156 (2022) 111980, https://doi.org/10.1016/j.rser.2021.111980.
[77] Z. Wu, P. Yang, Q. Li, W. Xiao, Z. Li, G. Xu, F. Liu, B. Jia, T. Ma, S. Feng, L. Wang, Microwave synthesis of Pt clusters on black TiO2 with abundant oxygen vacancies for efficient acidic electrocatalytic hydrogen evolution, Angewandte Chemie 135 (2023) e202300406, https://doi.org/10.1002/ange.202300406.
[78] J. Chen, Z. Ding, C. Wang, H. Hou, Y. Zhang, C. Wang, G. Zou, X. Ji, Black anatase titania with ultrafast sodium-storage performances stimulated by oxygen vacancies, ACS Appl. Mater. Interfaces 8 (2016) 9142–9151, https://doi.org/10.1021/acsami.6b01183.
[79] J. Dong, J. Han, Y. Liu, A. Nakajima, S. Matsushita, S. Wei, W. Gao, Defective black TiO2 synthesized via anodization for visible-light photocatalysis, ACS Appl. Mater. Interfaces 6 (2014) 1385–1388, https://doi.org/10.1021/am405549p.
[80] X. Liu, B. Hou, G. Wang, Z. Cui, X. Zhu, X. Wang, Black titania/graphene oxide nanocomposite films with excellent photothermal property for solar steam generation, J. Mater. Res. 33 (2018) 674–684, https://doi.org/10.1557/jmr.2018.25.
[81] H. Zhang, J. Cai, Y. Wang, M. Wu, M. Meng, Y. Tian, X. Li, J. Zhang, L. Zheng, Z. Jiang, J. Gong, Insights into the effects of surface/bulk defects on photocatalytic hydrogen evolution over TiO2 with exposed {001} facets, Appl. Catal. B 220 (2018) 126–136, https://doi.org/10.1016/j.apcatb.2017.08.046.
[82] Z. Wang, C. Yang, T. Lin, H. Yin, P. Chen, D. Wan, F. Xu, F. Huang, J. Lin, X. Xie, M. Jiang, Visible-light photocatalytic, solar thermal and photoelectrochemical properties of aluminium-reduced black titania, Energy Environ. Sci. 6 (2013) 3007–3014, https://doi.org/10.1039/C3EE41817K.

[83] E. Jalali, S. Maghsoudi, E. Noroozian, A novel method for biosynthesis of different polymorphs of TiO2 nanoparticles as a protector for Bacillus thuringiensis from Ultra Violet, Sci. Rep. 10 (2020) 426, https://doi.org/10.1038/s41598-019-57407-6.
[84] Y. Ding, Y. Wu, T. Zhang, L. Tao, X. Liu, X. Liu, L. Hu, T. Hayat, A. Alsaedi, S. Dai, Colorful TiO2-x microspheres cooperating with titanium Schiff base complex for efficient visible light photocatalysts, Catal. Today 335 (2019) 550–556, https://doi.org/10.1016/j.cattod.2019.03.004.
[85] J.C. Parker, R.W. Siegel, Calibration of the Raman spectrum to the oxygen stoichiometry of nanophase TiO2, Appl. Phys. Lett. 57 (1990) 943–945, https://doi.org/10.1063/1.104274.
[86] X. Chen, S.S. Mao, Titanium dioxide nanomaterials: synthesis, properties, modifications, and applications, Chem. Rev. 107 (2007) 2891–2959, https://doi.org/10.1021/cr0500535.
[87] G. Zeng, K.-K. Li, H.-G. Yang, Y.-H. Zhang, Micro-Raman mapping on an anatase TiO2 single crystal with a large percentage of reactive (001) facets, Vib. Spectrosc. 68 (2013) 279–284, https://doi.org/10.1016/j.vibspec.2013.08.012.
[88] M. Salari, K. Konstantinov, H.K. Liu, Enhancement of the capacitance in TiO2 nanotubes through controlled introduction of oxygen vacancies, J. Mater. Chem. 21 (2011) 5128–5133, https://doi.org/10.1039/C0JM04085A.
[89] W.F. Zhang, Y.L. He, M.S. Zhang, Z. Yin, Q. Chen, Raman scattering study on anatase TiO2 nanocrystals, J. Phys. D: Appl. Phys. 33 (2000) 912–916, https://doi.org/10.1088/0022-3727/33/8/305.
[90] D. Bersani, P.P. Lottici, T. Lopez, X.-Z. Ding, A. Raman, Scattering Study of PbTiO3 and TiO2 Obtained by Sol-Gel, J. Solgel. Sci. Technol. 13 (1998) 849–853, https://doi.org/10.1023/A:1008602718987.
[91] B.D. Viezbicke, S. Patel, B.E. Davis, D.P. Birnie III, Evaluation of the Tauc method for optical absorption edge determination: ZnO thin films as a model system, Physica Status Solidi 252 (2015) 1700–1710, https://doi.org/10.1002/pssb.201552007.
[92] X. Pan, M.-Q. Yang, X. Fu, N. Zhang, Y.-J. Xu, Defective TiO 2 with oxygen vacancies: synthesis, properties and photocatalytic applications, Nanoscale 5 (2013) 3601–3614, https://doi.org/10.1039/C3NR00476G.
[93] F. Chen, T. Ma, T. Zhang, Y. Zhang, H. Huang, Atomic-level charge separation strategies in semiconductor-based photocatalysts, Adv. Mater. 33 (2021) 2005256, https://doi.org/10.1002/adma.202005256.
[94] Y. Zou, K. Yang, Q. Chen, H. Wang, X. Meng, Molten salt construction of stable oxygen vacancies on TiO2 for enhancement of visible light photocatalytic activity, RSC. Adv. 8 (2018) 36819–36825, https://doi.org/10.1039/C8RA07543C.
[95] X. Jiang, Y. Zhang, J. Jiang, Y. Rong, Y. Wang, Y. Wu, C. Pan, Characterization of oxygen vacancy associates within hydrogenated TiO2: a positron annihilation study, J. Phys. Chem. C 116 (2012) 22619–22624, https://doi.org/10.1021/jp307573c.
[96] L.-Y. Lin, S. Kavadiya, X. He, W.-N. Wang, B.B. Karakocak, Y.-C. Lin, M.Y. Berezin, P. Biswas, Engineering stable Pt nanoparticles and oxygen vacancies on defective TiO2 via introducing strong electronic metal-support interaction for efficient CO2 photoreduction, Chem. Eng. J. 389 (2020) 123450, https://doi.org/10.1016/j.cej.2019.123450.
[97] X. Ma, X. Wang, L. Xu, F. Chen, Oxygen vacancy clusters enriched TiO2 with low Pt content for superior photocatalytic activity, Catal. Lett. 152 (2022) 2585–2589, https://doi.org/10.1007/s10562-021-03855-7.
[98] Md.A. Alam, R.K. Bishwas, S. Mostofa, S.A. Jahan, Crystallographic phase stability of nanocrystalline polymorphs TiO2 by tailoring hydrolysis pH, S. Afr. J. Chem. Eng. 49 (2024) 73–85, https://doi.org/10.1016/j.sajce.2024.04.007.
[99] M. Bellardita, G. Camera-Roda, V. Loddo, F. Parrino, L. Palmisano, Coupling of membrane and photocatalytic technologies for selective formation of high added value chemicals, Catal. Today 340 (2020) 128–144, https://doi.org/10.1016/j.cattod.2018.09.024.
[100] A. Barzagan (Ed.), Photocatalytic Water and Wastewater Treatment, IWA Publishing, 2022, https://doi.org/10.2166/9781789061932.
[101] M. Mirzaei, B. Dabir, M. Dadvar, M. Jafarikojour, Photocatalysis of phenol using a spinning disc photoreactor immobilized with TiO2 nanoparticles: hydrodynamic modeling and reactor optimization, Ind. Eng. Chem. Res. 56 (2017) 1739–1749, https://doi.org/10.1021/acs.iecr.6b03204.
[102] H.G. Tompkins, S. Tasic, J. Baker, D. Convey, Spectroscopic ellipsometry measurements of thin metal films, Surface Interface Anal. 29 (2000) 179–187, https://doi.org/10.1002/(SICI)1096-9918(200003)29:3<179::AID−SIA701>3.0.CO;2-O.
[103] Z. Li, P. Beck, D.A.A. Ohlberg, D.R. Stewart, R.S. Williams, Surface properties of platinum thin films as a function of plasma treatment conditions, Surf. Sci. 529 (2003) 410–418, https://doi.org/10.1016/S0039-6028(03)00015-3.
[104] P.S. Tóth, G. Szabó, G. Bencsik, G.F. Samu, K. Rajeshwar, C. Janáky, Peeling off the surface: Pt-decoration of WSe2 nanoflakes results in exceptional photoelectrochemical HER activity, SusMat 2 (2022) 749–760, https://doi.org/10.1002/sus2.86.
[105] T.S. Natarajan, M. Thomas, K. Natarajan, H.C. Bajaj, R.J. Tayade, Study on UV-LED/TiO2 process for degradation of Rhodamine B dye, Chem. Eng. J. 169 (2011) 126–134, https://doi.org/10.1016/j.cej.2011.02.066.
[106] D.C. Hurum, A.G. Agrios, K.A. Gray, T. Rajh, M.C. Thurnauer, Explaining the enhanced photocatalytic activity of Degussa P25 mixed-phase TiO2 using EPR, J. Phys. Chem. B 107 (2003) 4545–4549, https://doi.org/10.1021/jp0273934.
[107] M. Utami, S. Wang, F.I. Fajarwati, S.N. Salsabilla, T.A. Dewi, M. Fitri, Enhanced Photodegradation of Rhodamine B Using Visible-Light Sensitive N-TiO2/rGO Composite, Crystals. (Basel) 13 (2023) 588, https://doi.org/10.3390/cryst13040588.
[108] T. Wu, G. Liu, J. Zhao, H. Hidaka, N. Serpone, Photoassisted degradation of dye pollutants. 5. self-photosensitized oxidative transformation of rhodamine B under visible light irradiation in aqueous TiO2 dispersions, J. Phys. Chem. B 102 (1998) 5845–5851, https://doi.org/10.1021/jp980922c.
[109] T. Watanabe, T. Takizawa, K. Honda, Photocatalysis through excitation of adsorbates. 1. Highly efficient N-deethylation of rhodamine B adsorbed to cadmium sulfide, J. Phys. Chem. 81 (1977) 1845–1851, https://doi.org/10.1021/j100534a012.
[110] M. Pica, S. Calzuola, A. Donnadio, P.L. Gentili, M. Nocchetti, M. Casciola, De-ethylation and cleavage of rhodamine B by a zirconium phosphate/silver bromide composite photocatalyst, Catalysts. 9 (2019) 3, https://doi.org/10.3390/catal9010003.
[111] F. Chen, J. Zhao, H. Hidaka, Highly selective deethylation of rhodamine B: adsorption and photooxidation pathways of the dye on the TiO2/SiO2 composite photocatalyst, Int. J. Photoenergy 5 (2003) 209–217, https://doi.org/10.1155/S1110662×03000345.
[112] N. Chang, J. Liu, Y. Ji, J. Liu, Y. Chen, Kinetic study of Rhodamine B degradation of electro-catalysis by TiO2/activated semi-coke composite as tiny electrode, J. Sol-Gel Sci. Technol. 106 (2023) 684–698, https://doi.org/10.1007/s10971-023-06087-w.
[113] Y. Gu, L. Zhao, M. Yang, Y. Xiong, Z. Wu, M. Zhou, J. Yan, Preparation and characterization of highly photocatalytic active hierarchical BiOX (X=Cl, Br, I) microflowers for rhodamine B degradation with kinetic modelling studies, J. Cent. South Univ. 24 (2017) 754–765, https://doi.org/10.1007/s11771-017-3477-x.
[114] W. Zhang, H. He, H. Li, L. Duan, L. Zu, Y. Zhai, W. Li, L. Wang, H. Fu, D. Zhao, Visible-light responsive TiO2-based materials for efficient solar energy utilization, Adv. Energy Mater. 11 (2021) 2003303, https://doi.org/10.1002/aenm.202003303.
[115] I. Katsounaros, W.B. Schneider, J.C. Meier, U. Benedikt, P. Ulrich Biedermann, A. A. Auer, K.J.J. Mayrhofer, Hydrogen peroxide electrochemistry on platinum: towards understanding the oxygen reduction reaction mechanism, Phys. Chem. Chem. Phys. 14 (2012) 7384–7391, https://doi.org/10.1039/C2CP40616K.
[116] J. Liu, G. Dong, J. Jing, S. Zhang, Y. Huang, W. Ho, Photocatalytic reactive oxygen species generation activity of TiO2 improved by the modification of persistent free radicals, Environ. Sci.: Nano 8 (2021) 3846–3854, https://doi.org/10.1039/D1EN00832C.
[117] S. Drdova, M. Giannakou, F. Jiang, L. Lin, D. Sivaraman, R. Toth, T. Graule, A. Braun, J. Ilavsky, I. Kuzmenko, J. Wang, Aerosol-assisted deposition for TiO2 immobilization on photocatalytic fibrous filters for VOC degradation, Front. Chem. 10 (2022) 887431, https://doi.org/10.3389/fchem.2022.887431.
[118] Y. Li, G. Lu, S. Li, Photocatalytic transformation of rhodamine B and its effect on hydrogen evolution over Pt/TiO2 in the presence of electron donors, J. Photochem. Photobiol. A 152 (2002) 219–228, https://doi.org/10.1016/S1010-6030(02)00210-1.
[119] A. Das, M.K. Adak, N. Mahata, B. Biswas, Wastewater treatment with the advent of TiO2 endowed photocatalysts and their reaction kinetics with scavenger effect, J. Mol. Liq. 338 (2021) 116479, https://doi.org/10.1016/j.molliq.2021.116479.
[120] A. Fujishima, X. Zhang, D.A. Tryk, TiO2 photocatalysis and related surface phenomena, Surf. Sci. Rep. 63 (2008) 515–582, https://doi.org/10.1016/j.surfrep.2008.10.001.
[121] C. Di Valentin, G. Pacchioni, A. Selloni, Reduced and n-type doped TiO2: nature of Ti3+ species, J. Phys. Chem. C 113 (2009) 20543–20552, https://doi.org/10.1021/jp9061797.
[122] J.J. Rueda-Marquez, I. Levchuk, P. Fernández Ibañez, M. Sillanpää, A critical review on application of photocatalysis for toxicity reduction of real wastewaters, J. Clean. Prod. 258 (2020) 120694, https://doi.org/10.1016/j.jclepro.2020.120694.